Comp. Meth. Civil Eng., Vol. 2, 2 (2011) 201-218

CMCE
Computational Methods in Civil Engineering

A multi-lined behavior simulation approach for liquefaction of earth-dam

S.A. Sadrnejad*

Department of Civil Engineering, K.N.Toosi University of Technology, Teheran, Iran

Received 6 August 2011; accepted in revised form 31 October 2011

Abstract

A few of the presented soil behavior models are capable of predicting the triggering and post liquefaction and also shear band mechanism through the soil media. The assessment of earth-dam body behavior as a soil structure made of cohesive soil in core and non-cohesive soil as the core supports, including water interaction at upstream through earthquake upon a multi-line constitutive equations is the aim of this paper. A multi-plane mechanism-based approach is successfully employed for assigning post-liquefaction displacement of earth-dam structures. This approach is derived from total stress procedures with two major advantages: 1) the triggering and post liquefaction response have been multi-lined into one analysis, and 2) the modeling of post liquefaction behavior is greatly improved. Analyses are performed in the time domain, allowing the imposed earthquake motion to affect both the triggering and post-liquefaction deformations. This Multi-plane based framework is employed to sum up the strength effects on integrated sampling planes and the resultant of this simulated multi-lined behavior is implemented at each finite element Gauss point. This multi-plane based model is also capable of predicting the effects of both induced and inherent anisotropy plus the rotation of principal stress/strain axes through the plastic behavior of both cohesive and non-cohesive soils. The approach is presented through the simulated of the case history as the response of the lower San Fernando dam to the 1971 San Fernando earthquake. The magnitude and pattern of the predicted displacements are shown to be in good agreement with the measured values.

Keywords: Multi-line model; Liquefaction; Earth-dam.

1. Introduction

In general, liquefaction susceptibility at a particular site is largely dictated by initial conditions of the site, including spatial distributions of soil density, permeability, degree of saturation, material fabric, and stress states. On the other side, about the shear failure of soil media, there are two approaches available for mechanical behaviour of geo-materials to estimate displacements: empirical equations and mechanics-based analyses. Empirical relationships are valuable as they directly include the intangible aspects of field response. They are derived from field observations, are often limited to specific topographic and

*Corresponding author.
E-mail address: sadrnejad@kntu.ac.ir

material conditions, and may be impractical for evaluating two-dimensional effects. Mechanics-based methods approximate plasticity of soil behaviour using numerical models. These models attempt to capture the physics of soil response, although their success is limited by inherent simplifications. These methods require some knowledge of soil properties, such as stiffness and strength change through plastic deformations. Mechanics-based approaches vary in complexity from equivalent-linear methods [1,2] to advanced effective stress models [3,4]. The accepted state of practice is often a three-phase total stress procedure:

- Triggering evaluation: Zones of liquefaction are predicted by comparing estimates of cyclic shear stress to the anticipated resistance to liquefaction. Equivalent linear techniques are often used. Triggering resistance is frequently based on empirical correlation and in-situ tests [5].
- Flow slide evaluation: If significance zones of liquefaction are predicted, the potential for a flow slide is evaluated using limit equilibrium techniques. The susceptibility to large deformations is found by assigning residual strengths of sampling planes to the liquefied zones and appropriate undrained strengths to non-liquefied material. If the safety factor is less than or near 1, large deformations are assumed.
- Displacement evaluation: Large but limited displacements may occur even if the structure has sufficient strength to maintain overall stability. These displacements accumulate during the earthquake and are a direct result of the continuing inertia loading. Techniques for estimating these displacements are often based on Newmark [6] and model the displacing soil as a rigid polygon block translating on a plane.

Current practice has many advantages, including wide experience and the relative simplicity of procedure and input. There are also drawbacks including the simple evaluation of triggering, the crude modelling of post-liquefaction mechanics, and the disjointed nature of the three-phase procedure. The approach presented below attempts to capitalize on the experience and understanding of current practice, while simulating the components of a total stress evaluation into a more coherent, rational multi-lined method.

The task of representing the overall stress tensor in terms of micro level stresses and the condition, number and magnitude of contact forces has long been the aim of numerous researchers Zienkewics [7].

A multi-plane model capable of predicting the plastic behavior of geo-material on sampling planes developed by the author [8,9]. In those models the hardening rule as function of scalar value of plastic shear strain could not see the full strain history in plasticity.

The concept of the proposed multi-line model, however, seems to be realistic and natural, physically meaningful and simple. According to this formulation which is based on a simple numerical integration, an appropriate connection between averaged micro and macro-mechanical behavior of material has been presented. The inclusion of the rotation of principal stress and strain axes, induced anisotropy and the possibility of supervising pre-failure behavior and even controlling any variation through the medium are the significant of the model.

Actually, multi-plane concept by defining the small continuum structural units as an assemblage of particles and voids that fill infinite spaces between the sampling planes, has appropriately justified the contribution of interconnection forces in overall macro-mechanics. Plastic deformations are assumed to occur due to sliding, separation/closing of the boundaries and elastic deformations are the overall responses of structural unit bodies. Therefore, the overall deformation of any small part of the medium is composed of total elastic response and an appropriate summation of sliding, separation/closing phenomenon under the current effective normal and shear stresses on sampling planes.

2. Strain distribution around a point

In general continuum mechanics, to define strain distribution at a point, the components simply are considered on the outer surface of a typical *dx, dy, dz* element. This method makes the solution to consider uniform and homogeneous strain distribution of nine components over the outer surface of such *dx, dy, dz* element on three perpendicular coordinate axes. There is a further consideration in addition to the requirement that displacements of a granular medium provided due to slippage/widening/closing between particles that make a contribution to the strain in addition to that from the compression of particles. Consider two neighbouring points on either side of the point of contact of two particles. These two points do not in general remain close to each other but describe complex trajectories. Fictitious average points belonging to the fictitious continuous medium can be defined which remain adjacent so as to define a strain tensor. The problem presents itself differently for disordered particles compared with ordered sphere of equal sizes. In this case small zones even may appear in which there is no relative movement of particles. This can lead to specific behaviour such as periodic instabilities known as slip-stick that creates non-homogeneity in strains and displacements.

The effects of non-homogeneity in mechanical behaviour of non-linear materials are very important and must somehow be considered. Furthermore, these non-homogeneities mostly are neglected in mechanical testing because strains and stresses are usually measured at the boundary of the samples and therefore have to be considered reasonably within whole volume.

Solving a non-linear problem, the mechanical behaviour depends strongly on stress/strain path as well as their histories. Upon these conditions, it may be claimed that the consideration of strain components along three perpendicular coordinate axes may not reflect the real historical changes during the loading procedure. In the most extreme case, the definition of a sphere shape element dr (instead of *dx, dy, dz* cube) carrying distributed strain similarly on its surface can reflect strain components on infinite orientation at a point when *dr* tends to zero.

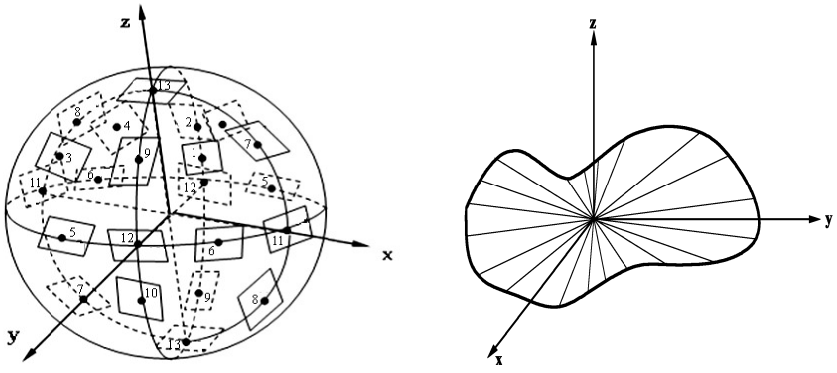

(a) (b)

Figure 1. (a) sphere elements; (b) typical deformed element.

The finite strain at any point in three dimensions by coordinates (*x, y, z*) relate to the displacements of the sides of an initial rectangular-coordinate box with sides of length *dx, dy*, and *dz* to form the three sides of a parallelepiped. This configuration of strain is established by considering the displacements of the corner points (*x, 0, 0*), (*0, y, 0*), and (*0, 0, z*). This kind of strain approach leads to define a (3×3) strain tensor including six components to present displacement gradient matrix at a node. Accordingly, any displacement and corresponding gradient have to be defined as independent components on three perpendicular coordinate axes.

Figure 1 shows sphere elements and a typical deformed shape of them. Obviously, there is a certain history of displacement on any random orientation through the element. These are abbreviated in three when a box -shape element is employed. To avoid not missing any directional information of strain, a spherical element carrying strain components over its surface, as tangent and normal to the surface must be employed. This form of strain certainly represents a better distribution includes all directional information. Certainly, to obtain the strain components as presented on planes around box element, strain variation is integrated over the sphere surface. However, a predefined numerical integration may be employed to ease the solution. Numerical integration generally simulates the smooth curved sphere surface to a composition of flat tangential planes make an approximated polygon to sphere surface. Any higher number of sampling planes, the approximated surface is more closed to sphere. Clearly, if the number of sampling planes is taken six, the approximated surface is the same as normal *dx, dy, dz* box element. In this research, the major deformations assumed to take place on sampling planes upon multi-line model and summed up rationally to make an over sphere surface of a point.

3. Muti-plane framework concept

Grains in a granular materials consisting of contacts and surrounding voids are particulate media that mostly are considered continuum for ease. The accurate behaviour of such particulate materials is to be investigated through micro-mechanics. However, the micro-mechanical behaviour of granular materials is therefore inherently discontinuous and heterogeneous. The macroscopic as an overall or averaged behaviour of granular materials is determined not only how discrete grains are arranged through medium, but also by what kinds of interactions are operating among them. To investigate the micro-mechanical behaviour of granular materials, certainly, the spatial distribution of contact points and orientation of grains must be identified. In engineering point of view, the main goal is to formulate macro-behaviour of granular materials in terms of micro-quantities. However, there exist two well-known theories that explain the relation between micro-fields and macro-fields as macro-micro relations, in a consistent manner as the average field theory and the homogenization theory.

For a granular material such as sand that supports the overall applied loads through contact friction, the overall mechanical response ideally may be described on the basis of micro-mechanical behaviour of grains interconnections. Naturally, this requires the description of overall stress, characterization of fabric, representation of kinematics, development of local rate constitutive relations and evaluation of the overall differential constitutive relations in terms of the local quantities. Representation the overall stress tensor in terms of micro level stresses and the condition, number and magnitude of contact forces has long been the aim of numerous researchers. Multi-plane framework by defining the small continuum structural units as an assemblage of particles and voids that fill infinite spaces between the sampling planes, has appropriately justified the contribution of interconnection forces in overall macro-mechanics. Upon these assumptions, plastic deformations are to occur due to sliding, separation/closing of the boundaries and elastic deformations are the overall responses of structural unit bodies. Therefore, the overall deformation of any small part of the medium is composed of total elastic response and an appropriate summation of sliding, separation/closing phenomenon under the current effective normal and shear stresses on sampling planes. These assumptions adopt overall sliding, separation/closing of inter-granular points of grains included in one structural unit are summed up and contributed as the result of sliding, separation/closing surrounding boundary planes. This simply implies yielding/failure or even ill-conditioning and bifurcation response to be possible over any of

the randomly oriented sampling planes. Consequently, plasticity control such as yielding should be checked at each of the planes and those of the planes that are sliding will contribute to nonlinear or plastic deformations. Therefore, the granular material mass has an infinite number of yield functions usually one for each of the planes in the physical space.

Figure 2 shows the arrangement of artificial polyhedron simulated by real soil grains. The created polyhedrons are roughly by 13 sliding planes, passing through each point in medium. The location of tip heads of normal to the planes defining corresponding direction cosines are shown on the surface of unit radius sphere.

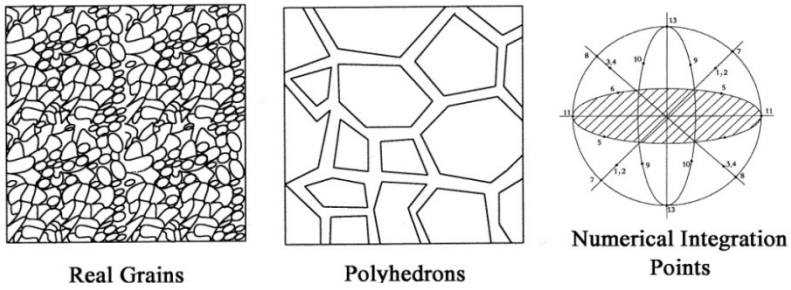

Figure 2. Soil grains, artificial polyhedrons, and sampling points.

In ideal case, the normal integration is considered as summing up the individual micro effects correspond to infinite number of micro sampling planes.

The orientation of the sampling planes and direction cosines of two perpendicular on plane coordinate axes and weighted coefficients for employed numerical integration rule and calculation of stress tensor of each plane are shown in Figure 3.

Plane NO		1	2	3	4	5	6	7	8	9	10	11	12	13
NORMAL AXIS	l_i	$\frac{\sqrt{3}}{3}$	$\frac{\sqrt{3}}{3}$	$-\frac{\sqrt{3}}{3}$	$-\frac{\sqrt{3}}{3}$	$\frac{\sqrt{2}}{2}$	$-\frac{\sqrt{2}}{2}$	$\frac{\sqrt{2}}{2}$	$-\frac{\sqrt{2}}{2}$	0	0	1	0	0
	m_i	$\frac{\sqrt{3}}{3}$	$-\frac{\sqrt{3}}{3}$	$\frac{\sqrt{3}}{3}$	$-\frac{\sqrt{3}}{3}$	$\frac{\sqrt{2}}{2}$	$\frac{\sqrt{2}}{2}$	0	0	$-\frac{\sqrt{2}}{2}$	$\frac{\sqrt{2}}{2}$	0	1	0
	n_I	$\frac{\sqrt{3}}{3}$	$\frac{\sqrt{3}}{3}$	$\frac{\sqrt{3}}{3}$	$\frac{\sqrt{3}}{3}$	0	0	$\frac{\sqrt{2}}{2}$	$\frac{\sqrt{2}}{2}$	$\frac{\sqrt{2}}{2}$	$\frac{\sqrt{2}}{2}$	0	0	1
W_i		$\frac{27}{840}$	$\frac{27}{840}$	$\frac{27}{840}$	$\frac{27}{840}$	$\frac{32}{840}$	$\frac{32}{840}$	$\frac{32}{840}$	$\frac{32}{840}$	$\frac{32}{840}$	$\frac{32}{840}$	$\frac{40}{840}$	$\frac{40}{840}$	$\frac{40}{840}$

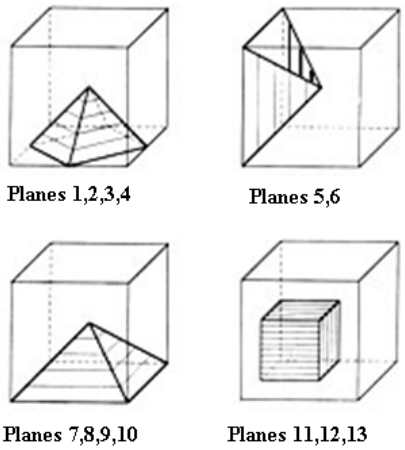

Figure 3. Direction cosines, weighted coefficient, Demonstration of 13 planes.

The application of any stress path is accompanied with the activities of some of the 13 defined planes at any point in the medium upon on plane stress increaments. Therefore, the values of strain on all the active planes are not necessarily the same. Some of these planes initiate deformations earlier than the others. These priorities and certain active planes can change due to any change of direction of stress path, a number of active planes may stop activity and some inactive ones become active and some planes may take over others with respect to the value of on plane stress increaments. Thus the framework is able to predict the mechanism of failure upon plane activities and exceeding a certain limit shear/normal strain.

3.1. Constitutive Equation for Sampling Points

In many instances, the scale of the microstructure is coarse enough to be out of the range of such specific considerations of slip theory, and the individual component blocks can be considered as a continuum with well-defined certain linear resistances and hardening/softening behaviour. In this research, the individual component blocks of the overall media deform collectively as a heterogeneous (but compatible in deformations with other blocks) assembly of continua, interacting with each other only through the boundary conditions applicable at their various interfaces.

The choice of 13 independent planes (Figure 3) for the solution of any three dimensional problem based on getting a good distribution of deformation mechanism through the media and avoiding huge computing time is a fair number. The orientation of the sampling planes as given by their direction cosines of normal axis and the weight coefficients for numerical integration rule are given in fist three and the last rows of Figure 3. The coefficients *Wi* choosing any number of sampling points, are simply calculated based on Gauss Quadrature numerical integration rule.

A coordinate system has been employed for each plane in such manner that one axis is perpendicular to the plane and the other two are laid on the plane as shown in Figure 4. Shear strain increments on each plane is considered as two component vectors on defined coordinate axes of plane. The presented coefficients *Wi* are acceptable for a first order tensor, that must be corrected for a second order tensor like stress or strain distribution over the surface of sphere. They must be multiplied by the ratio of area for each sampling plane on sphere.

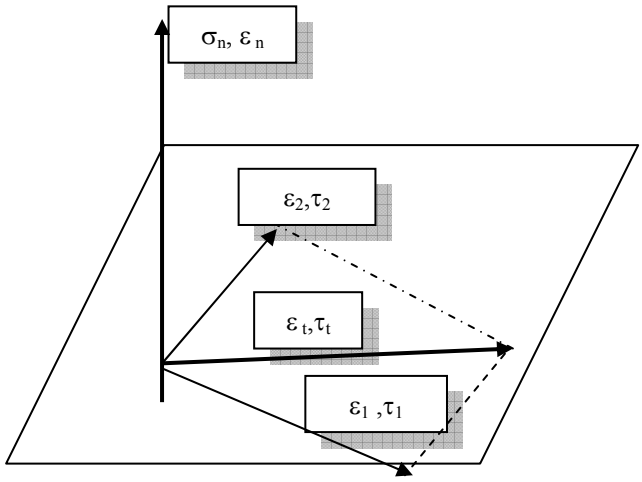

Figure 4. On plane stress/strain components.

4. Stress and strain vectors

In all that follows { } denotes a (9) 6-element column vector and [ ] a matrix. The superscript *T* indicates the transposed array. The effective stress vector, the strain vector, the vector equivalent of the Kronecker delta tensor are defined as follows:

$$\begin{aligned}\{\varepsilon\} &= \{\varepsilon_{11} \quad \varepsilon_{22} \quad \varepsilon_{33} \quad \varepsilon_{12} \quad \varepsilon_{21} \quad \varepsilon_{13} \quad \varepsilon_{31} \quad \varepsilon_{23} \quad \varepsilon_{32}\}^T \\ \{\sigma\} &= \{\sigma_{11} \quad \sigma_{22} \quad \sigma_{33} \quad \sigma_{12} \quad \sigma_{21} \quad \sigma_{13} \quad \sigma_{31} \quad \sigma_{23} \quad \sigma_{32}\}^T\end{aligned} \tag{1}$$

The stress vector is transferred on all planes to establish the plasticity of each one. These transfers are done by multiplying related transitive matrixes which are derived from their direction cosines. There are three stress components, the first is normal stress component σ_n and others τ_1 and τ_2 are tangential, on each plane.

$$\begin{Bmatrix}\tau_1 \\ \tau_2 \\ \sigma_n\end{Bmatrix}_i = [T_i]\cdot\{\sigma\}, \quad \tau = \sqrt{\tau_1^2 + \tau_2^2} \tag{2}$$

$[T_i]$ is the transitive matrix of plane i and defined as:

$$[T_i] = \begin{bmatrix} L_{x_i'x} & L_{x_i'y} & L_{x_i'z} \\ L_{y_i'x} & L_{y_i'y} & L_{y_i'z} \\ L_{z_i'x} & L_{z_i'y} & L_{z_i'z} \end{bmatrix} \cdot \begin{bmatrix} l_i & 0 & 0 & m_i & 0 & n_i & 0 & 0 & 0 \\ 0 & m_i & 0 & 0 & l_i & 0 & 0 & n_i & 0 \\ 0 & 0 & n_i & 0 & 0 & 0 & l_i & 0 & m_i \end{bmatrix} \tag{3}$$

Based on description of local axes, and also the relations for transition of stress tensor to an arbitrary plane, we must multiply the transferred matrix by a rotation matrix to be presented in our local axes on each plane. Therefore, *L* is the rotation matrix, and x_i', y_i' and z_i' are local axes of plane i and

$$\begin{aligned} S_{x_i} &= l_i \cdot \sigma_{11} + m_i \cdot \sigma_{12} + n_i \cdot \sigma_{13} \\ S_{y_i} &= l_i \cdot \sigma_{21} + m_i \cdot \sigma_{22} + n_i \cdot \sigma_{23} \\ S_{z_i} &= l_i \cdot \sigma_{31} + m_i \cdot \sigma_{32} + n_i \cdot \sigma_{33} \end{aligned} \tag{4}$$

S_{x_i}, S_{y_i} and S_{z_i} are stress component of plane i in global directions. Then, the derivatives of σ_n and τ are:

$$\sigma_{n,\sigma_i} = \begin{Bmatrix} l_i \cdot l_i \\ m_i \cdot m_i \\ n_i \cdot n_i \\ m_i \cdot l_i \\ m_i \cdot l_i \\ n_i \cdot l_i \\ n_i \cdot l_i \\ n_i \cdot m_i \\ n_i \cdot m_i \end{Bmatrix}, \quad \tau_{,\sigma_i} = \left(\frac{1}{\tau}\right) \cdot \begin{Bmatrix} S_{x_i} \cdot l_i - \sigma_n \cdot l_i^2 \\ S_{y_i} \cdot m_i - \sigma_n \cdot m_i^2 \\ S_{z_i} \cdot n_i - \sigma_n \cdot n_i^2 \\ S_{x_i} \cdot m_i - \sigma_n \cdot m_i \cdot l_i \\ S_{y_i} \cdot l_i - \sigma_n \cdot m_i \cdot l_i \\ S_{x_i} \cdot n_i - \sigma_n \cdot n_i \cdot l_i \\ S_{z_i} \cdot l_i - \sigma_n \cdot n_i \cdot l_i \\ S_{y_i} \cdot n_i - \sigma_n \cdot n_i \cdot m \\ S_{z_i} \cdot m_i - \sigma_n \cdot n_i \cdot m_i \end{Bmatrix} \tag{5}$$

Generally the stress components on each plane are independent. It suffices to say that this deficiency does not produce significant error which can be omitted by calibration. Also, stress ratio of each plane defined as follows:

$$\zeta = \frac{\tau}{\sigma_n} \tag{6}$$

4.1. Multi-lined behaviour approach

The framework of the multi-lined behaviour approach is a typical numerical solution technique. A finite element continuum model is used, although the approach can be adapted to other methods such as finite point or even finite difference methods. General three dimensional structures are discretized into elements, masses are lumped at nodal points, and constitutive relationships and properties are assigned.

An explicit solution scheme is used where the dynamic equations of equilibrium are satisfied for each mass at every time step. This allows changes in the material stiffness, strength, or stress of an element to be rationally considered: each element strains dynamically in response to out-of balance forces. This scheme requires small time steps, often less than 0.0001 seconds, but easily models nonlinear and large strain response.

The analysis prior to liquefaction is similar to the equivalent linear method. A multi-line elastic-plastic constitutive model is used in combination with Rayleigh stiffness-proportional viscous damping. Elastic module is estimated from the maximum shear modulus, max G, and a modulus reduction factor, MRF. But unlike equivalent linear methods, the Multi-lined approach is not iterative. Appropriate values of MRF and damping are selected through calibration. Suitable values of undrained strength, S_u, are also assigned and affected by the changes in MRF. Changes in pore pressure prior to liquefaction are not directly included, but can be approximated through a reduction in volumetric stiffness.

For the first linear behavior, the stress~ strain can be written as follows:

$$0 \le \varepsilon_t \le \varepsilon_{t1} \Rightarrow \begin{Bmatrix} \varepsilon_n \\ \varepsilon_t \end{Bmatrix} = \begin{bmatrix} \frac{1}{\gamma} & \frac{\beta_1}{\alpha_1} \\ 0 & \frac{1}{\alpha_1} \end{bmatrix} \begin{Bmatrix} \sigma_n \\ \tau \end{Bmatrix}, \; D = \alpha_1 \gamma_1 \begin{bmatrix} \frac{1}{\alpha_1} & -\frac{\beta_1}{\alpha_1} \\ 0 & \frac{1}{\gamma} \end{bmatrix} \tag{7-1}$$

$$0 \le \varepsilon_t \le \varepsilon_{t1} \Rightarrow \begin{Bmatrix} \varepsilon_n \\ \varepsilon_t \end{Bmatrix} = \begin{bmatrix} \frac{1}{\gamma} & \frac{\beta_1}{\alpha_1} \\ 0 & \frac{1}{\alpha_1} \end{bmatrix} \begin{Bmatrix} \sigma_n \\ \tau \end{Bmatrix}, \; D = \alpha_1 \gamma_1 \begin{bmatrix} \frac{1}{\alpha_1} & -\frac{\beta_1}{\alpha_1} \\ 0 & \frac{1}{\gamma} \end{bmatrix} \tag{7-2}$$

The line parameters α_1, β_1 and γ are the slopes for three stress/strain components shown in Figure. These slopes for the second, third and forth linear behavior are α_2, β_2, γ for the second and also α_n, β_n and γ are for the n^{th} line, respectively and similar relation can be written as follow:

$$\varepsilon_{t1} \le \varepsilon_t \le \varepsilon_{t2} \Rightarrow C = \begin{bmatrix} \frac{1}{\gamma} & \frac{\beta_2}{\alpha_2} \\ 0 & \frac{1}{\alpha_2} \end{bmatrix}, D = \alpha_2 \gamma \begin{bmatrix} \frac{1}{\alpha_2} & -\frac{\beta_2}{\alpha_2} \\ 0 & \frac{1}{\gamma} \end{bmatrix} \tag{8-1}$$

$$\left.\begin{aligned}
&\varepsilon_{t1} \le \varepsilon_t \le \varepsilon_{t2} \Rightarrow \sigma_n = \gamma\varepsilon_n - \gamma\ \beta_1\varepsilon_{t1} - \gamma\beta_2\left(\varepsilon_t - \varepsilon_{t1}\right)\\
&\tau = \alpha_1\varepsilon_t + \alpha_2\left(\varepsilon_t - \varepsilon_{t1}\right) \Rightarrow \varepsilon_n = \frac{\sigma_n}{\gamma} + \varepsilon_t\left(\beta_1 - \beta_2\right) + \frac{\beta_2}{\alpha_2}\tau + \beta_2\varepsilon_{t1}\left(1 - \frac{\alpha_1}{\alpha_2}\right)\\
&\varepsilon_t = \frac{1}{\alpha_2}\tau + \varepsilon_{t1}\left(1 - \frac{\alpha_1}{\alpha_2}\right)
\end{aligned}\right\} \qquad (8\text{-}2)$$

$$\Rightarrow \begin{Bmatrix}\varepsilon_n\\ \varepsilon_t\end{Bmatrix} = \begin{bmatrix}\frac{1}{\gamma} & \frac{\beta_2}{\alpha_2}\\ 0 & \frac{1}{\alpha_2}\end{bmatrix}\begin{Bmatrix}\sigma_n\\ \tau\end{Bmatrix} + \begin{Bmatrix}\varepsilon_{t1}\left(\beta_1 - \beta_2\right)\\ \varepsilon_{t1}\left(1 - \frac{\alpha_1}{\alpha_2}\right)\end{Bmatrix}$$

For any line with negative slope the relation is as follow:

$$\varepsilon_{t2} \le \varepsilon_t \le \varepsilon_{t3} \Rightarrow C = \begin{bmatrix}\frac{1}{\gamma} & \frac{\beta_3}{\alpha_3}\\ 0 & \frac{1}{\alpha_3}\end{bmatrix}, D = \alpha_3\gamma\begin{bmatrix}\frac{1}{\alpha_3} & -\frac{\beta_3}{\alpha_3}\\ 0 & \frac{1}{\gamma}\end{bmatrix} \qquad (9\text{-}1)$$

$$\left.\begin{aligned}
&\varepsilon_{t2} \le \varepsilon_t \le \varepsilon_{t3} \Rightarrow \sigma_n = \gamma\varepsilon_n - \gamma\beta_1\varepsilon_{t1} - \gamma\beta_2\left(\varepsilon_{t2} - \varepsilon_{t1}\right) - \gamma\beta_3\left(\varepsilon_t - \varepsilon_{t2}\right)\\
&\tau = \alpha_1\varepsilon_t + \alpha_3\left(\varepsilon_t - \varepsilon_{t1}\right) \Rightarrow \varepsilon_n = \frac{\sigma_n}{\gamma} + \varepsilon_{t1}\left(\beta_1 - \beta_2\right) + \frac{\beta_2}{\alpha_3}\tau - \beta_2\frac{\alpha_1}{\alpha_3}\varepsilon_{t1} + \beta_2\varepsilon_{t2}\\
&\varepsilon_t = \frac{1}{\alpha_3}\tau - \frac{\alpha_1}{\alpha_3}\varepsilon_{t1} + \varepsilon_{t2}
\end{aligned}\right\} \qquad (9\text{-}2)$$

$$\Rightarrow \begin{Bmatrix}\varepsilon_n\\ \varepsilon_t\end{Bmatrix} = \begin{bmatrix}\frac{1}{\gamma} & \frac{\beta_2}{\alpha_3}\\ 0 & \frac{1}{\alpha_3}\end{bmatrix}\begin{Bmatrix}\sigma_n\\ \tau\end{Bmatrix} + \begin{Bmatrix}\varepsilon_{t1}\left(\beta_1 - \beta_2\right) - \frac{\beta_2\alpha_1}{\alpha_3}\varepsilon_{t1}\\ -\frac{\alpha_1}{\alpha_3}\varepsilon_{t1} + \varepsilon_{t2}\end{Bmatrix}$$

For any horizontal line with zero slopes the relation is as follows:

$$\varepsilon_{t3} \le \varepsilon_t \Rightarrow C = \begin{bmatrix}\frac{1}{\gamma} & 0\\ 0 & \frac{1}{\alpha_4}\end{bmatrix}, D = \alpha_4\gamma_1\begin{bmatrix}\frac{1}{\alpha_4} & 0\\ 0 & \frac{1}{\gamma}\end{bmatrix} \qquad (10\text{-}1)$$

$$\left.\begin{aligned}
&\varepsilon_{t3} \le \varepsilon_t \Rightarrow \sigma_n = \gamma\varepsilon_n - \gamma\beta_1\varepsilon_{t1} - \gamma\beta_2(\varepsilon_{t2} - \varepsilon_{t1}) - \gamma\beta_3(\varepsilon_{t3} - \varepsilon_{t2}) \\
&\tau = \alpha_1\varepsilon_{t1} + \alpha_3(\varepsilon_{t3} - \varepsilon_{t2}) + \alpha_4(\varepsilon_t - \varepsilon_{t3}) \\
&\Rightarrow \varepsilon_n = \frac{\sigma_n}{\gamma} + \beta\varepsilon_{t1} + \beta_2(\varepsilon_{t2} - \varepsilon_{t1}) + \beta_1(\varepsilon_{t3} - \varepsilon_{t2}) \\
&\varepsilon_t = \frac{1}{\alpha_4}\tau - \frac{\alpha_1}{\alpha_4}\varepsilon_{t1} - \frac{\alpha_3}{\alpha_4}(\varepsilon_{t3} - \varepsilon_{t2}) + \varepsilon_{t3}
\end{aligned}\right\} \tag{10-2}$$

$$\Rightarrow \begin{Bmatrix}\varepsilon_n \\ \varepsilon_t\end{Bmatrix} = \begin{bmatrix}\frac{1}{\gamma} & 0 \\ 0 & \frac{1}{\alpha_4}\end{bmatrix}\begin{Bmatrix}\sigma_n \\ \tau\end{Bmatrix} + \begin{Bmatrix}\beta_1\varepsilon_{t1} + \beta_2(\varepsilon_{t2} - \varepsilon_{t1}) + \beta_1(\varepsilon_{t3} - \varepsilon_{t2}) \\ -\frac{\alpha_1}{\alpha_4}\varepsilon_{t1} - \frac{\alpha_3}{\alpha_4}(\varepsilon_{t3} - \varepsilon_{t2}) + \varepsilon_{t3}\end{Bmatrix}$$

In a general form, ε_0 can be defined as initial strain for a linear behavior and the corresponding stress/strain relation assumed as follows:

$$\begin{Bmatrix}\varepsilon_n \\ \varepsilon_t \\ \varepsilon'_t\end{Bmatrix} = \begin{bmatrix}C_{11} & 0 & 0 \\ 0 & C_{22} & 0 \\ 0 & 0 & C_{33}\end{bmatrix}\begin{Bmatrix}\sigma_n \\ \tau_1 \\ \tau_2\end{Bmatrix} + \{\varepsilon_0\} \tag{11}$$

Transforming 3x3 plane compliance matrix into 6x6 at global coordinate and summing up by numerical integration to provide compliance matrix at a point, it can be computed as follows:

$$\hat{C}_i = T_i.C_i.T_i^T \tag{12}$$

$$C = 8\pi\sum w_i.\hat{C}_i \tag{13}$$

4.2. Triggering of liquefaction

Triggering of liquefaction is evaluated by tracking the dynamic shear and normal stress on the predefined sampling planes, within each gauss point of element. The cyclic pulse, as changes in stress levels of six components are transferred to each sampling plane and are computed at every time step and added up to that existed prior to the earthquake. The irregular stress history of each plane is interpreted as a succession of a small increment effect of percentage of a cycle, with the contribution of each fraction of cycle determined by its maximum value of τ_{cyc} . This definition of cyclic loading is shown schematically in Figure 5.

A cumulative damage technique combines the effect of each half cycle. This approach converts the non-uniform τ_{cyc} history into an equivalent series of uniform stress cycles. The amplitude of the uniform history is arbitrarily set to τ_{max}, which is the value of τ_{15} required to cause liquefaction in 15 cycles. This transformation uses the cyclic strength curve as a weighting curve as shown in Figure 6 and described below. The approach is similar to work developed at the University of California at Berkeley [10].

1. For each half cycle, use weighting curve to find N_{liq}, the number of uniform cycles of τ_{cyc} required to cause liquefaction.
2. Multiply N_{liq} by 2 to find the number of half cycles of τ_{cyc} needed to cause liquefaction.
3. Compute relative contribution of current half cycle to liquefaction: $1/(2\times N_{liq})$.

4. Compute equivalent number of cycles based on 15 cycles to liquefaction: $N_{eq} = 15/(2 \times N_{liq})$.
5. Sum the effect of each half cycle, ΣN_{eq} . Liquefaction is triggered when $\Sigma N_{eq} \geq 15$.

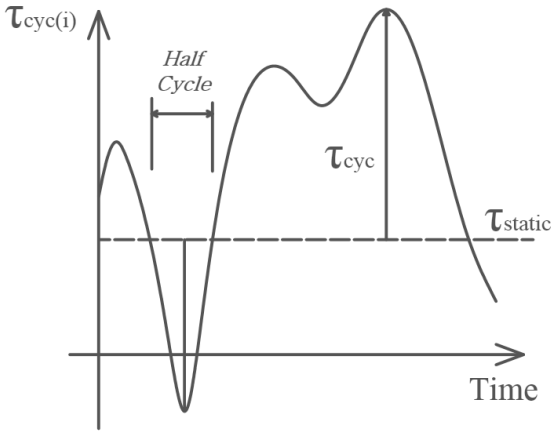

Figure 5. Half cycle and τ_{cyc}.

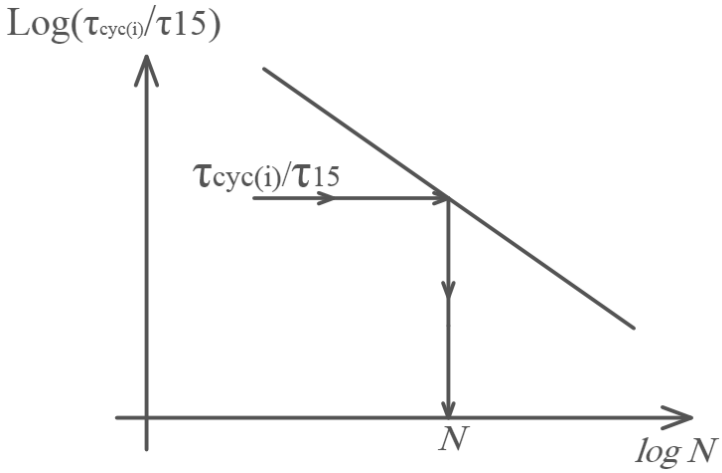

Figure 6. Weighting curve.

An idealized stress-strain curve showing the onset of liquefaction is given in Figure 7. The Multi-lined method attempts to capture this behaviour by continuously evaluating τ_{cyc} rather than just peak values. Triggering is assumed when the current value of τ_{cyc} is sufficient to bring ΣN_{eq} to 15 at the end of the next half cycle. This causes triggering to begin when the element is under shear stress, rather than at a stress reversal. The direction of τ_i can also been considered as it is often more likely to initiate liquefaction when the cyclic pulse and the static bias are in the same direction.

Since the triggering of each sampling plane in gauss points of element are evaluated separately, liquefaction first occurs in the most susceptible planes in the areas and then spreads with further dynamic loading in a realistic manner. The effects of progressive liquefaction, including load shedding and base isolation, are rationally considered.

A reduced stiffness and a residual strength is specified when liquefaction is triggered on a sampling plane. The constitutive model is also modified so that unloading occurs along a stiffer path than loading, as shown in Figure 7 and Figure 8. This multi-line model permits the accumulation of displacement with each cycle while still maintaining a simple elastic-plastic formulation. Due to the large hysteretic damping component, the viscous damping coefficients in the liquefied elements are also reduced.

Anisotropy is incorporated by making the strength a function of the major principal stress direction according to strength ellipsoid. Residual strength on different sampling planes are specified for known stress paths, usually corresponding to compression and shear on each plane. An interpolation function derived from three triaxial standard test results are then used to build up strength ellipsoid to present the distribution of strength with principal stress direction at any point. The importance of anisotropy during monotonic loading has been well demonstrated by hollow cylinder torsion tests [11]. Undrained strengths of water-pluviated sand can vary by factors of 3 to 5 or more depending on the stress path.

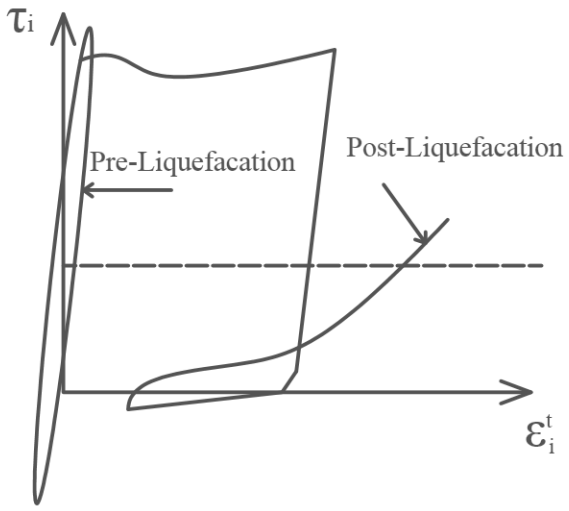

Figure 7. Idealized stress-strain behaviour.

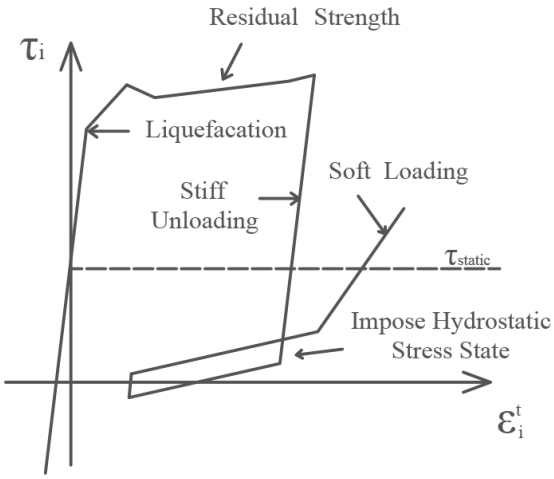

Figure 8. Multi-lined approach model.

Another feature of liquefied behaviour is the occurrence of high pore pressure and loss of effective stress at shear stress reversals. This is simulated by imposing a hydrostatic stress state whenever a liquefied element experiences a on plane shear stress reversal. The lateral total stresses are set equal to the vertical stress and the on plane shear stresses are removed: $\sigma_{xx} = \sigma_{yy}$, $\sigma_{xx} = \sigma_{zz}$, and τ_i.=0 while i=1~13. Imposing these stresses momentarily removes all shear stress from the element, as is the case when the excess pore pressure ratio, r_u, equals 100%.

The simple multi-line model shown on Figure 4 causes the on plane shear stresses to increase quickly after a stress reversal.

This representation is adequate when on plane strains accumulate primarily in one global direction, such as may occur for elements with a pronounced static bias. A softened loading modulus can also be imposed immediately after a on plane stress reversal to more accurately model symmetric loading.

The approach described above assumes a rapid transition into liquefied behaviour. This may not always occur, especially for denser materials. Contrary to intuition, assuming a quick transition into liquefied behaviour may lead to an under prediction of the displacements. Early liquefaction can introduce base isolation effects that limit the final extent of liquefaction. Such possibilities must be considered when evaluating analyses.

4.3. Simulation of Lower San-Fernando dam

The Lower San Fernando dams are located in southern California, roughly 30 kilometres north of downtown Los Angeles. The dams were built as part of the Los Angeles Aqueduct system, with construction beginning in 1912 for the lower dam. This dam was built using variations of the hydraulic fill method. This method yielded a central clayey core with highly stratified shells consisting of sand, silty sand, and clay. The sandy layers have a representative fines content of about 25%. The Lower San Fernando dam was about 44 metres in height, founded on up to 11 metres of alluvium, and originally had slopes of 2.5:1. A rolled fill berm with a 4.5:1 slope was added to the downstream face in 1940. This berm creates a 6-metre-wide bench at an elevation 15 metres below the crest (Figures 9). The mechanical properties of dam body are presented in Table 1.

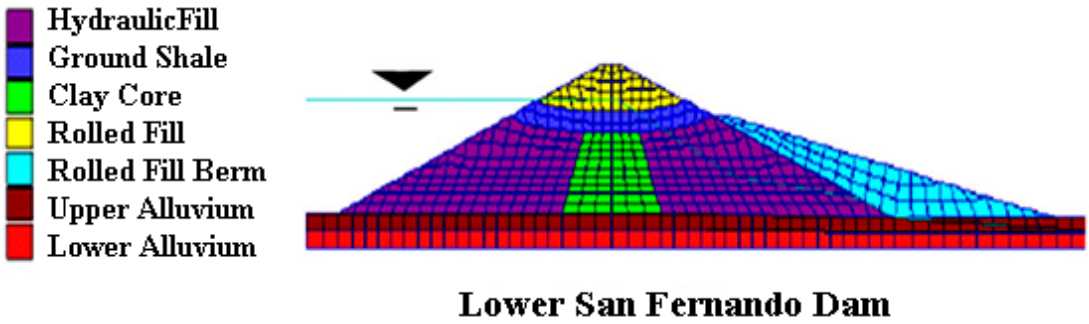

Figure 9. Finite element mesh (central portion) and material zones.

Table 1. Selected input properties for critical hydraulic fill zones.

Lower San Fernando Dam					
	Upstream	Downstream		Upstream	Downstream
Pre-Liquefaction			**Post-Liquefaction**		
$(N_1)_{60}$	11.5	12.5	$(N_1)_{60-cs}$	13.5	14.5
$(N_1)_{60-cs}$	13	14	S_r/σ'_{vo}		
$K_{2\,max}$	43	43	• Simple Shear	0.13	0.15
			• Compression	0.5	0.5
MRF	0.14	0.14	Shear Modulus		
S_u	≃ Drained Strength	≃ Drained Strength	• $G_{loading}$	$S_r/0.05$	$S_r/0.05$
			• $G_{unloading}$	$10 \times G_{loading}$	$10 \times G_{loading}$

4.4. Observed seismic response

The San Fernando earthquake occurred on February 9, 1971, had an M_w of 6.6, and an epicentre about 11 km from the dams. Peak ground accelerations at the site were estimated to be around 0.6g (Figures 10). The response of the lower dam was dominated by the near catastrophic slide of the upstream face and crest. The 11 metres of freeboard prior to the earthquake were reduced to a fragile 1.5 metres. An extensive field investigation found that liquefaction of the fill near the base of the upstream shell was responsible for the slide [12].

The slide extended 45 to 60 metres into the reservoir. Large blocks of intact fill were transported by the liquefied soil. An evaluation of the crest seismoscope record indicates the slide occurred about 20 to 30 seconds after the earthquake shaking had stopped.

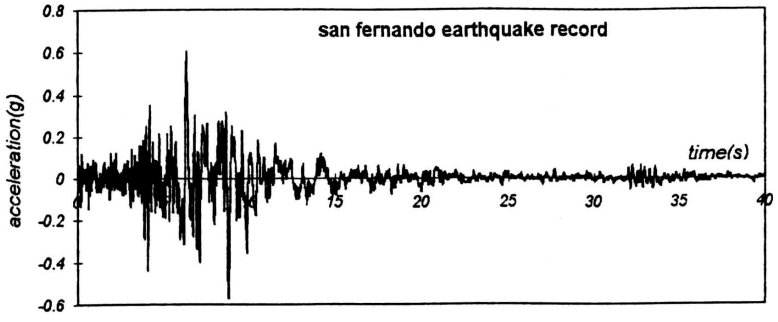

Figure 10. Acceleration time history.

Tension cracks and evidence of shear failure were seen in the inlet conduit at the base of the embankment. Liquefaction was suggested by sand boils below the toe and increased water levels in the three standpipe piezometers. Water overflowed from two of the piezometers.

4.5. Description of model results

The initial static analyses were performed using a hyperbolic model. The embankment was constructed in layers and the reservoir load was added. Once the grid reached equilibrium, the constitutive model was changed, dynamic properties were assigned, and the earthquake motion was applied to the base. Liquefaction was permitted throughout the saturated hydraulic fill zone, but not in the other embankment zones or the foundation.

Two features distinguish the actual response of the Lower San Fernando dam: (1) limited displacements during the earthquake, and (2) a near catastrophic failure of the upstream slope following the earthquake. Figure 11(a) shows the estimated displacement vectors at the end of the earthquake. Predicted crest displacements are less than 0.2 metres and downstream slope displacements are less than about 0.3 metres. This is generally consistent with expectations. Figure 6(a) shows fewer liquefied zones than was anticipated, perhaps due to base isolation effects. Liquefaction at the bottom of the upstream shell coincides with observations. The predicted liquefaction near the upstream face was not observed in the field, and likely resulted from the simplifying assumption of $K = 1$. Seed used high values of K near the slopes in his evaluation [13].

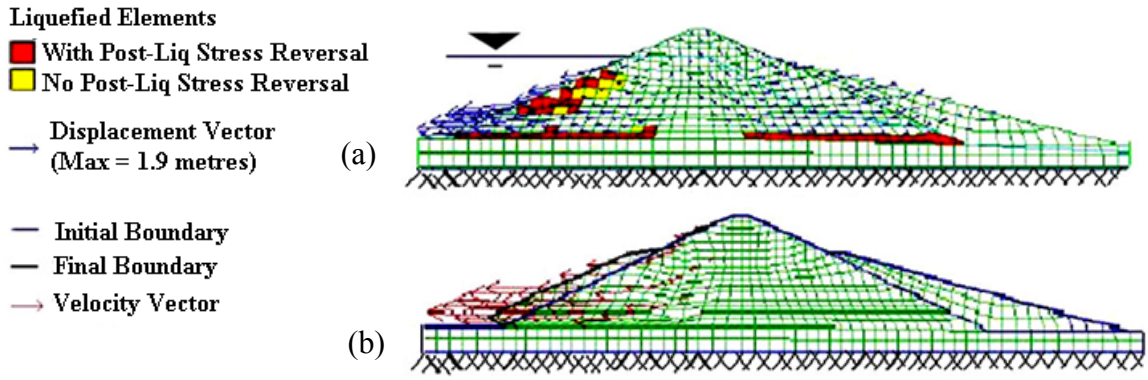

Figure 11. Analysis results for Lower San Fernando dam. (a) liquefied zones and displacement vectors at the end of earthquake; (b) displacing shape from post-earthquake analysis.

Figure 12(a) shows developed pore water pressure contours at triggering liquefaction pointing the liquefied zone. The effective mean stress contours conforming to the developed pore water pressure contours are presented in Figure 12(b). The failed Gauss points contours and shear bands passing through the progressed failed Gauss points are shown in Figure 12(c).

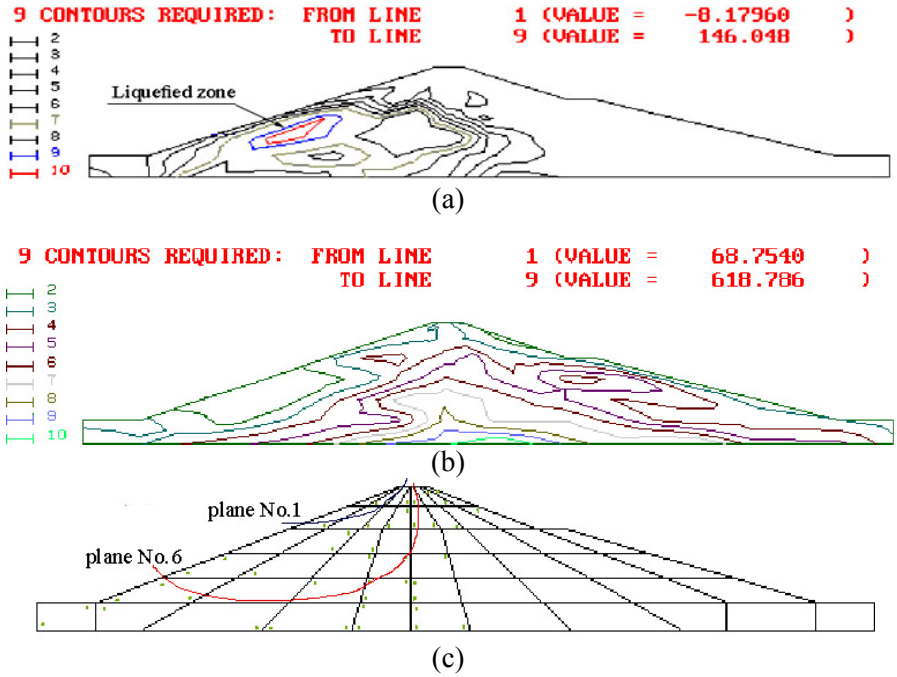

Figure 12. Post-earthquake analysis result for Lower San Fernando dam. (a) build up pore water pressure contours; (b) effective mean stress contours; (c) failed Gauss point's contours.

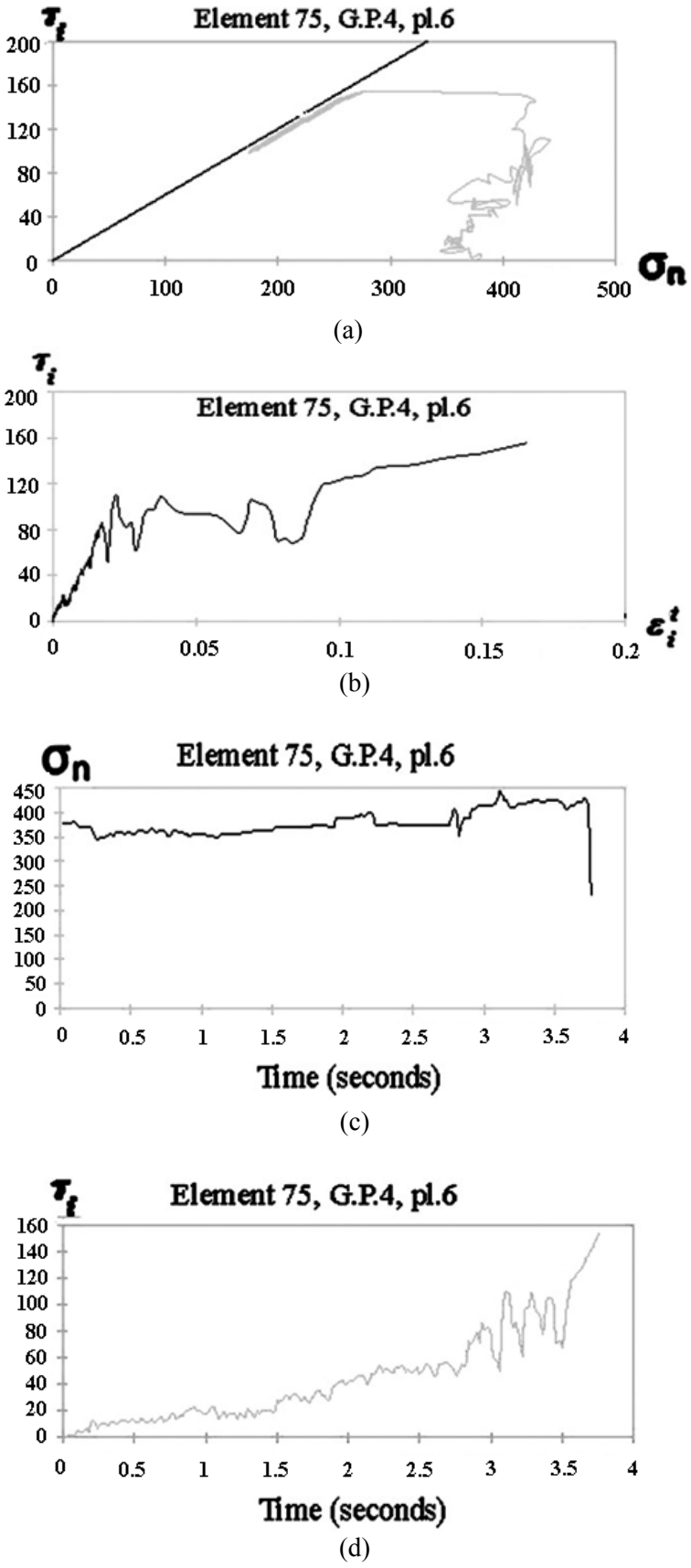

(a)

(b)

(c)

(d)

Figure 13. Stress variation of the failed Gauss point number 4 in element 75, plane number 6. (a) stress path; (b) the variation of stress vs. strain; (c) stress time histories of the first failed plane No. 6; (d) Stress time histories of the first failed plane No. 6.

According to the presented results in Figure 12, the post-earthquake instability may have resulted from excess pore pressure flowing from loose liquefied zones into denser material, or from the formation of water lenses beneath continuous low-permeability layers. This latter possibility was approximately modelled by continuing the analysis after the earthquake motion had stopped. The strength of liquefied material at the base of the upstream and downstream shells was slowly reduced. The analysis proceeded until the grid became highly distorted. The resulting deformations and velocity vectors are shown in Figure 11(b). This pattern indicates a substantial and progressing failure of the upstream shell, and relative stability of the downstream shell. This behaviour is extremely complex and difficult to predict using total stress approaches. Proper investigations fall within the domain of effective stress analyses.

The stress path of the failed Gauss points number 4 in element 75, plane number 6 is shown in Figure 13(a). The shear stress versus shear strain variation of this failed plane is shown if Figure 13(b). Figures 13(c) and 13(d) show on plane stress components up to triggering liquefaction.

5. Conclusions

A multi-lined behaviour approach is presented which simulates the pre- and post-liquefaction behaviour of sand. The model permits simultaneous evaluation of triggering and post-liquefaction displacement. It directly considers the reduced stiffness, strength anisotropy, and occurrence of high pore pressure ($r_u = 100\%$) in liquefied soils.

Triggering of liquefaction is evaluated on the nearest sampling planes orientation through liquefied elements, permitting deformation of zones of liquefaction to develop with loading in a rational manner. The effects of progressive liquefaction leading to failure, including base isolation and load shedding, are directly considered.

The response of the Lower San Fernando dams to the 1971 San Fernando earthquake was simulated using the method. Reasonable to good agreement was obtained between field observations and the analyses.

Critical input parameters include N_{liq}, residual strength in simple shear, viscous damping coefficients, direction of loading, and frequency content of the input motion. The highly non-linear nature of the analysis necessitates some level of sensitivity study whenever the approach is used.

The multi-lined approach combined with multi-line framework is a powerful and useful analytic tool, but it retains the inherent limitations of finding on plane parameters from global test results as a complicated approach. Effective stress analyses are required to properly investigate complex behaviour, such as was observed at the Lower San Fernando dam.

References

[1] I.M. Idriss, J. Sun, *User's Manual for SHAKE91*, Center for Geotechnical Modeling, UC Davis., 1992.

[2] Itasca, *FLAC, Fast Lagrangian Analysis of Continua, Version 3.40 User's Guide*, Itasca Consulting Group Inc., 1998.

[3] M. Beaty, P.M. Byrne, An effective stress model for predicting liquefaction behavior of sand, *Geotechnical Earthquake Engineering and Soil Dynamics III*, ASCE, 1 (1998) 766 - 777.

[4] W.D.L. Finn, M. Yogendrakumar, N. Yoshida, *Response of 2D embankment systems to seismic loading – program TARA-3*, Soil Mechanics Series, University of British Columbia, Canada, 1986.

[5] T.L. Youd, I.M. Idriss, *Proceedings of the NCEER Workshop on Evaluation of Liquefaction Resistance of Soils*, Report No. NCEER-97-0022, Multidisciplinary Center for Earthquake Engineering Research, 1998.

[6] N.M. Newmark, Effects of earthquakes on dams and embankments, *Geotechnique*, Vol. 15, 2 (1965) 139-160.

[7] O.C. Zienkiewicz, G.N. Pande, Time dependent multilaminate model of rocks, *Int. J. Num. Anal. Methods in Geomechanics,* 1 (1977) 219-247.

[8] S.A. Sadrnezhad, G.N. Pande, A multilaminate model for sand, *Proceeding of 3rd International symposium on Numerical Models in Geomechanics*, NUMOG-III, Niagara Falls, Canada, (May. 8-11, 1989).

[9] S.A. Sadrnezhad, A multilaminate, elastic-plastic model for liquefaction of saturated sand, *Proceeding of the Third International Conference on Seismology and Earthquake Engineering*, Iran, (May. 17-19, 1999) 561-568.

[10] K.L. Lee, K. Chan, Number of equivalent significant cycles in strong motion earthquakes, *Proceedings of the International Conference on Microzonation for Safer Construction Research and Application*, 2 (1972) 609-627.

[11] Y.P. Vaid, S. Sivathayalan, Fundamental factors affecting liquefaction susceptibility of sands, *Proceedings of the International Workshop, Physics and Mechanics of Soil Liquefaction*, Baltimore, Balkema, (1999).

[12] H.B. Seed, K.L. Lee, I.M. Idriss, F. Makdisi, Analysis of the slides in the San Fernando dams during the earthquake of Feb. 9, 1971, *Report No. EERC 73-2*, EERC and UC Berkeley, 1973.

[13] H.B. Seed, R.B. Seed, L.F. Harder, H.-L. Jong, Re-evaluation of the slide in the lower San Fernando dam in the earthquake of Feb. 9, 1971, *Report No. UCB/EERC-88/04*, EERC and UC Berkeley, 1988.